PHYSICAL REVIEW B VOLUME 50, NUMBER 15 15 OCTOBER 1994-I

Thermal-mismatch-strain relaxation in epitaxial CaF_2, BaF_2/CaF_2, and $PbSe/BaF_2/CaF_2$ layers on Si(111) after many temperature cycles

H. Zogg, S. Blunier, A. Fach, C. Maissen, and P. Müller
AFIF (Arbeitsgemeinschaft für Industrielle Forschung) at Swiss Federal Institute of Technology, ETH-Teil Technopark, CH-8005 Zürich, Switzerland

S. Teodoropol and V. Meyer
Physics Institute, University of Zürich, CH-8057 Zürich, Switzerland

G. Kostorz
Institute of Applied Physics, Swiss Federal Institute of Technology, ETH Hönggerberg, CH-8093 Zürich, Switzerland

A. Dommann
Neutechnikum Buchs, CH-9470 Buchs, Switzerland

T. Richmond
Institute of Physics, University of Basel, CH-4056 Basel, Switzerland

(Received 10 May 1994; revised manuscript received 11 July 1994)

The thermal mismatch strain in stacks containing PbSe, BaF_2, and/or CaF_2 on Si(111) substrates is relieved by the glide of dislocations in the principal $\langle 110\rangle\{100\}$ glide system. The strain in the $BaF_2(111)$ and $CaF_2(111)$ buffer layers is relaxed at room temperature regardless of whether they form the top layer in the stack or are overgrown by other layers. PbSe (as well as $Pb_{1-x}Sn_xSe$ and PbTe) top layers are capable of relieving the strain induced by the thermal-expansion mismatch even at 77 K, and after many temperature cycles between room temperature and 77 K. Even after 1400 such cycles, plastic relaxation still occurs on each cycle. The x-ray rocking curves, typically 150–190 arc sec wide, do not broaden on cycling. The total cumulative plastic deformation of the layer corresponds to as much as 400%. After the first few thermal cycles, no new thermal-strain-relieving dislocations are created, but the existing ones move back and forth on the same atomic glide planes with each cycle.

I. INTRODUCTION

Much work has been devoted to the problem of understanding the mechanisms of stress relaxation of epitaxial layers on lattice-mismatched substrates. Misfit dislocations form during or after growth if the layer has exceeded the critical coherency thickness. In most cases, a large number of these dislocation lines extends through a threading end up to the surface. Very high densities of these threading ends are frequently observed for typical layer thicknesses.[1] Significant improvements were made in recent years in decreasing these densities by using strained-layer superlattices or graded buffer layers.[2,3] However, in principle, there is no need for threading parts to form: lattice mismatch strain can be relaxed by a network of dislocations lying completely in the interface or in the interior of the layer without any threading ends reaching the surface. Such lattice-mismatched epitaxial layers free of dislocations at the surface would of course be ideal for electronic applications.

The situation changes if there is also a mismatch in the *thermal* expansion coefficients between substrate and layer. Stresses build up on cooling from growth temperature to room temperature (RT). If these stresses cannot relax by some mechanism, they can lead to delamination of the film for "weak" interfaces, while strong interfacial bonds may lead to cracks.

If the stresses induced by the thermal mismatch can relax through glide of dislocations, these dislocations have to glide along *inclined* glide planes across the whole layer. If the glide planes are parallel to the interface only, strain relaxation through movement of dislocations is not possible since the resolved shear stress is zero.[4] Dislocations with inclined glide planes may nucleate at the surface, become misfit dislocations after glide to the interface, and leave a surface step behind. In the ideal case, no additional defects are formed by these moving dislocations. This mechanism, or more precisely the resulting surface steps, has been observed for CaF_2 layers on Si(111) using atomic force microscopy (AFM),[5,6] and in lead chalcogenide (PbSe) layers on Si(111) with scanning tunneling microscopy (STM).[7,8] Similar results have been obtained by Mathet *et al.*[9,10] and by Nguyen-Van-Dau *et al.*[11] who also performed detailed transmission electron microscopy (TEM) studies. The primary system is $\langle 110\rangle\{100\}$ for PbSe as well as for CaF_2 and BaF_2. Owing to the (111) symmetry, a terraced surface structure with surface steps along the three symmetric $\langle 110\rangle$ directions forms (see Fig. 1). Knowing the difference in thermal expansions between the layers and the substrate

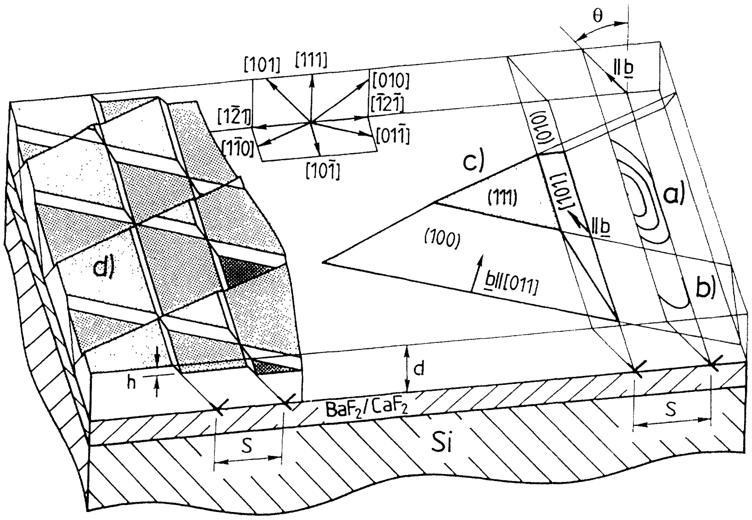

FIG. 1. Schematic drawing of nucleation (a) and glide of thermal-misfit-strain-relieving dislocations (b), glide planes and Burgers vectors of the ⟨110⟩{100} glide system for (111) oriented layers (c), and the resulting surface terrace morphology (d).

and analyzing the step heights and distances, the amount of relaxation can be calculated.[5–8]

These epitaxial narrow-gap compound semiconductor layers on Si substrates are of interest for the fabrication of infrared focal plane arrays for thermal imaging applications. We chose narrow-gap lead chalcogenides like PbSe and $Pb_{1-x}Sn_xSe$ rather than the well-known $Hg_{1-x}Cd_xTe$ for this purpose because of easier epitaxy.[12–14] The sensors are fabricated in the narrow-gap layer. The Si substrate serves as a support for bump bonding to a two-dimensional Si readout signal processing chip without any constraint in size due to a thermal expansion mismatch. Alternately, the Si substrate may contain this electronics itself.

An epitaxial group-IIA fluoride buffer layer is needed for compatibility reasons in order to obtain the desired high-quality epitaxy of the sensor narrow-gap material. This buffer typically consists of a thin CaF_2 layer whose thickness is between 30 and 200 Å, followed by a ≈2000-Å-thick BaF_2 layer. Some of the relevant properties of these materials are listed in Table I.

IV-VI materials, especially PbS, $Pb_{1-x}Sn_xSe$, or $Pb_{1-x}Sn_xTe$, are soft. Misfit dislocations in such epitaxial layers on Si, which relieve the large thermal mismatch strain easily, glide across the layers along the main glide planes, which are included by 54.5° with respect to the surface. The dislocations in the fluoride buffer layers can glide, too, but glide is not as easy as in the IV-VI layers. Dislocation climb is not expected to have any significance under the conditions encountered in this work.[15]

In the following, an attempt is made to get a better understanding of the relevant thermal-mismatch-strain relaxation mechanisms in the stacks by using already known data for single layers as well as new measurements. In infrared sensor applications, the sensors are operated at cryogenic temperatures while they are stored at RT. They have to withstand a large number of thermal cycles. We therefore investigated the change of the properties of the stacks, especially for the PbSe layers, as a function of the number of temperature cycles between RT and liquid-nitrogen temperature. Up to 1400 such cycles were performed.

II. EXPERIMENTAL

The layers were grown in a two-chamber molecular-beam epitaxy (MBE) apparatus onto 3-in. Si(111) wafers

TABLE I. Relevant material constants of various semiconductors and IIA insulators.

Material	Lattice constant at 300 K (Å)	Thermal-expansion coefficient (300 K) (10^{-6}/K)	Band-gap energy (77 K) (eV)	Elastic constants (300 K) c_{11} (GPa)	c_{12} (GPa)	c_{44} (GPa)	A[a]
Si	5.431	2.6	1.1	166	64	79	0.45
CaF_2	5.464	19.1		165	45	34	0.96
BaF_2	6.200	19.8		90	42	26	0.89
PbSe	6.124	19.4	0.18	124	19	17	1.16
$Pb_{1-x}Sn_xSe$ (x = 0–0.2)	6.124–6.06		0.18–0				
PbTe	6.462	19.8	0.22	10.8	0.77	1.34	1.09

[a] $A=-\epsilon_\perp/\epsilon_\parallel=2(c_{11}+2c_{12}-2c_{44})/(c_{11}+2c_{12}+4c_{44})$ for (111) orientation.

using resistively heated crucibles. The Si wafers were cleaned using either the Shiraki technique, or a final RT cleaning with HF in methanol in a dry N_2 box attached to the load-lock chamber. Details are described elsewhere.[6,8]

The grown layers were analyzed with different techniques. Strains were measured at different temperatures with x-ray diffraction (XRD) and RBS (Rutherford backscattering spectrometry) channeling. While RBS allows one to determine to some extent the strain at different depths of a layer, XRD as used in the present work yielded a mean value averaged over the layer thickness.

With XRD, the Bond technique[16] was used to determine the rhombohedral distortion ϵ_r by measuring the exact lattice plane distances for the symmetrical (333) and asymmetrical (531) or (422) reflections. If the lattice constants for unstrained samples were already known exactly, θ-2θ measurements were used, too, since they yield more accurate strain values relative to a known lattice constant, and can be done much faster.

For RBS channeling angular-yield spectra, a high-precision rotational stage was employed in order to measure the strain-induced angular deviations of low-indexed off-axis crystal directions. Relative angular differences (e.g., between the [110] directions of the undistorted substrate with respect to the corresponding direction of the overlayers) as well as absolute angle measurements (exact determination of the angle between two differently inclined lattice directions of the same layer) were performed.[17]

IIA fluorides are extremely sensitive to charged-particle irradiation. Strains induced by the He ions (spot size ≈ 1 mm^2) during the RBS measurements are already detectable at doses as low as 1 μC. In addition, continued irradiation with doses of a few tens of μC causes distortions ϵ_r up to 0.2%.[18] The location of the impinging focused He beam has to be changed frequently. At first glance, PbSe seems to be less sensitive to He^+ irradiation. When performing angular scans, the $X_{\min}$ (minimum backscattering yield in the channeled direction) remains stable, suggesting no radiation damage effects. However, the strain determined on the same irradiated areas behaves differently on temperature change compared to areas irradiated for the first time: pronounced irradiation hardening occurs. A new unirradiated area was therefore chosen for each spectrum. For the XRD measurements, we did not observe such effects, and reproducibility was obtained without any problems.

Transmission electron microscopy proved to be rather difficult to apply because of the charge sensitivity of IIA fluorides. STM or AFM were performed in air. High-resolution x-ray diffraction (HRXRD) was employed for rocking-curve measurements using a Bartels monochromator[19] which permits measurement of any lattice plane of any material.

III. MICROSCOPIC PICTURE OF GLIDING MISFIT DISLOCATIONS TO RELIEVE THE THERMAL STRAIN

As already described, misfit dislocations glide along inclined $\{100\}$ main glide planes and leave behind a surface step along a $\langle 110 \rangle$ direction. However, it is not known if these strain-relieving dislocations glide through the whole stack, or stop at the first obstacle or interface they have to cross. It seems reasonable that a dislocation loop originating at the top PbSe layer becomes a misfit dislocation at the PbSe/BaF_2 interface since PbSe grows type B with respect to BaF_2 [the lattice orientation is rotated 180° about the (111) surface normal], and its growth mode is by three-dimensional nucleation. For the BaF_2/CaF_2 interface where neither lattice type nor orientation change, and BaF_2 grows two dimensionally on CaF_2,[20] the situation is different. The vast majority of the *lattice*-misfit-relieving dislocations have their Burgers vectors in the interface plane; they are therefore sessile.[5,10] Whether thermal-strain-relieving dislocations can glide through such a dense network of dislocations is not known. In addition, TEM Moiré pattern analysis showed that threading dislocations in BaF_2/CaF_2 stacks on Si(111) can also have Burgers vectors parallel to the interface.[9,10,21]

Figures 2(a) and 2(b) show a TEM and a STM image of a PbSe layer, respectively. Both images have a comparable magnification. Note that TEM images the threading dislocations only, while the contrast of the STM picture is mainly due to the surface steps created by the thermal misfit dislocations.

When changing the temperature only slightly, the threading ends of the thermal misfit dislocations will move in order to relieve the thermally induced strain. For larger temperature changes, new dislocations are formed. In Fig. 2(c), the same surface as in Fig. 2(b) is imaged, but after a cooldown to 77 K. Clearly, the density of surface step lines is much higher. The same effect is observed after a heating cycle.[8]

IV. EXPERIMENTAL DETERMINATION OF THE STRAIN RELAXATION

A. CaF_2 on Si(111)

The lattice constant of CaF_2 is 0.6% larger than that of Si at RT and 2.4% larger at 750 °C, a typical growth temperature. The critical thickness h_c for generation of misfit dislocations is about 2 nm according to Matthews's theory.[22] Above h_c, the compressive strain relaxes following approximately a $1/d$ dependence. This strain vs thickness behavior at growth temperature is indicated with a solid line in Fig. 3.

On cooling down to RT, the lattice misfit shrinks to 0.6%. Assuming that the layer is strained elastically during cooldown (without any plastic strain relaxation) the solid curve shifts upwards by the amount $\int \Delta\alpha \, dT$ (dashed line in Fig. 3) where $\Delta\alpha$ is the difference in the thermal expansion coefficient between CaF_2 and Si. The predicted strain becomes tensile as soon as the layer thickness exceeds about 30 nm. Such behavior, i.e., no plastic strain relaxation after growth on cooldown, is found, for example, for ZnSe layers on GaAs substrates.[23] For CaF_2 on Si, plastic strain relaxation occurs even much below the growth temperature. The thermal equilibrium (tensile) strain value at RT is again given by

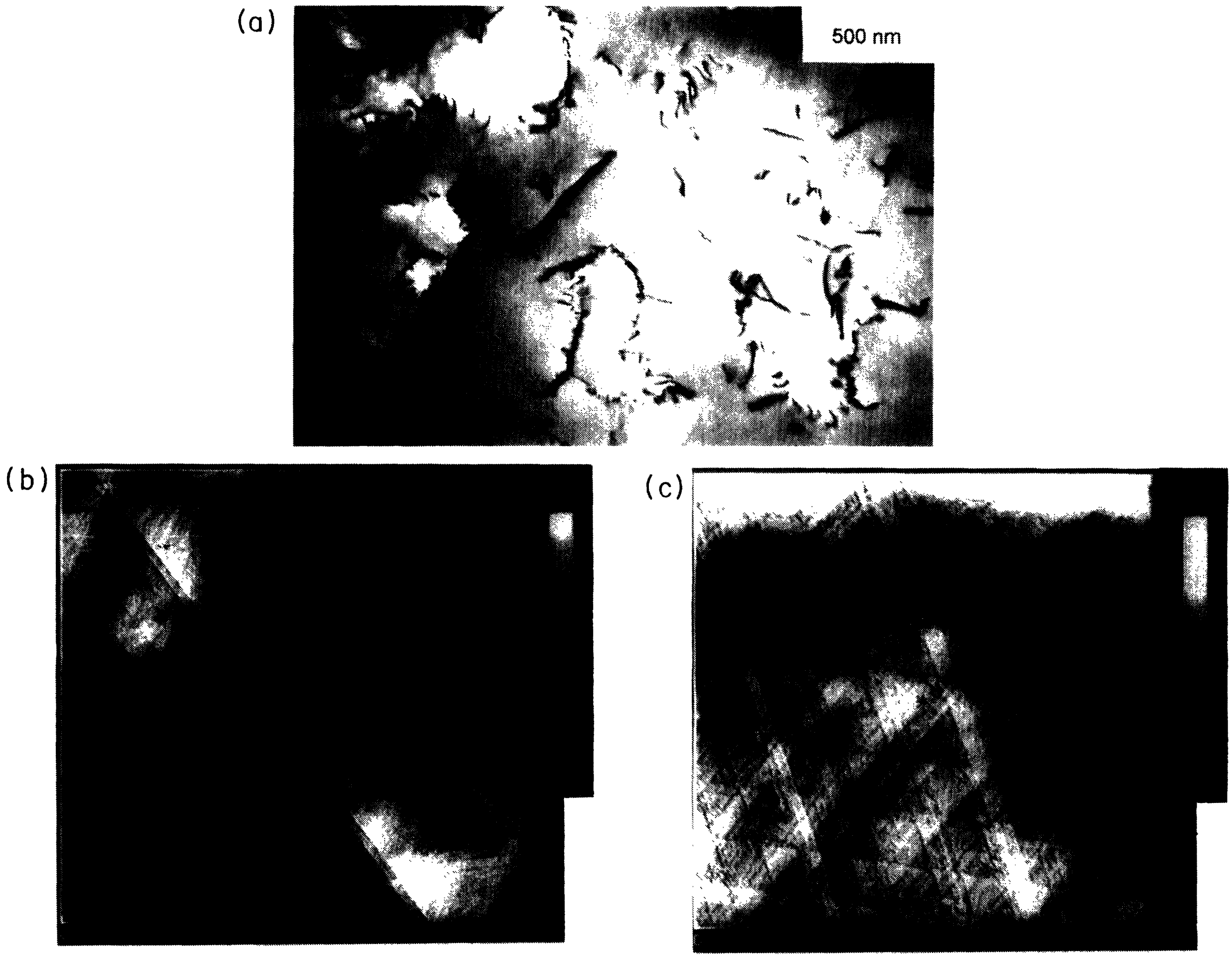

FIG. 2. (a) TEM image of a 0.2-μm-thick PbSe layer dissolved from the $BaF_2/CaF_2/Si(111)$ substrate. The main contrast is from threading dislocations. (b) STM image of a 2-μm-thick PbSe layer on $BaF_2/CaF_2/Si(111)$. The straight slip steps run along the three $\langle 011 \rangle$ directions, the intercepts of the $\{100\}$ glide planes with the surface. (c) Same sample as in (b), but after a temperature cycle down to 77 K.

Matthews's theory, and is drawn as the dash-dotted line in Fig. 3 for layers which are under tensile strain. Of course, the strain in thermal equilibrium should follow the dash-dotted line as soon as it is lower than the strain predicted without plastic relaxation. This behavior is indeed qualitatively observed: a near-zero or even compressive strain at very small thicknesses, a maximum in the range 200–500 Å, and again decreasing tensile strain for thicker layers. However, the layers have not relaxed completely to the equilibrium value. For more quantitative agreement, a frictional term may be taken into account, as has been done for SrF_2 layers on Si(111), and for CaF_2 layers on Si(111) with thicknesses larger than 200 Å by Schowalter and Li,[24] using adjustable parameters. The experimental points of that work[25] are included in the figure. They are in agreement with our strain determinations.[26]

B. BaF_2/CaF_2 stacks on Si(111)

1. Strain state at room temperature

The residual strain as a function of the BaF_2 layer thickness in BaF_2/CaF_2 stacks with fixed thickness of the CaF_2 part is plotted in Fig. 4. New as well as previously published values[27] are included. The strain relaxes approximately proportionally to $1/d$, but the absolute values predicted by Matthews's theory are much lower. The layers are not in thermal equilibrium; pronounced frictional forces seem to hinder further relaxation.

2. Depth profile

Typical stacks consisting of about 100 Å CaF_2 and 2000 Å BaF_2 were investigated. Using the RBS channeling technique, it is possible to deduce a depth profile of strains. The strain in the BaF_2 part is uniform within the measurement accuracy (20%) across the whole BaF_2 layer while the strain in the thin CaF_2 part is about six times higher than in the BaF_2 part.[28]

These results are verified using XRD. From the measured widths of the BaF_2 lines ($\Delta\theta \approx 0.1°$), the maximum strain variation across the layer thickness is deduced to be below 0.1%. The tensile strain in the thin CaF_2 part was determined from precision measurements of the (422) line. The results are included in Fig. 3 (open circles): The tensile strain of the buried CaF_2 layer is comparable

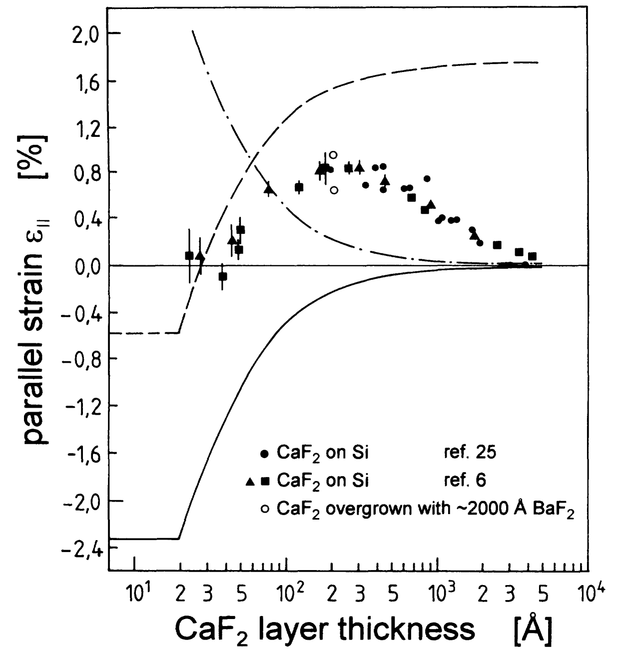

FIG. 3. Parallel strains $\epsilon_{\parallel}$ vs layer thickness for $CaF_2(111)$ layers on Si(111) substrates grown at 750 °C. Solid curve: calculated equilibrium strain at growth temperature; dashed curve: calculated strain after cooldown to RT assuming elastic deformation only; dash-dotted curve: calculated equilibrium strain at RT if plastic deformation is allowed after growth.

to the strain measured for the free CaF_2 layers. The BaF_2 layer, therefore, does not affect, within the uncertainty of the data, the strain relief in the CaF_2. Dislocations relieving thermal misfit strain are able to move in the buried CaF_2 layer, too, and their creation and movement is not appreciably hindered by the BaF_2 overlayer.

3. Strain state above and below room temperature

Since the thermal mismatch strain relaxes through dislocation movement after growth on cooldown to RT, temperature cycling between RT and higher temperatures must also lead to plastic deformation. If the layers were completely pinned to the substrate and deformed elastically only, the changes of the lattice spacing parallel to the surface $a_{\parallel}$ should follow exactly that of Si and lead to a strain parallel to the interface $\epsilon_{\parallel}(T) = -\int \Delta\alpha\, dT$, while the change in the lattice spacings perpendicular to the interface $\Delta a_{\perp} = a_{\perp}(T) - a_{\perp}(20\,°C)$ is given by[27]

$$\Delta a_{\perp}(T)/a_{\perp}(20°\ C) \approx (1+A)\int \Delta\alpha\, dT\ ,$$

where $A = -\epsilon_{\perp}/\epsilon_{\parallel}$ is determined by the elastic constants (Table I).

XRD measurements in the symmetric orientations, which measure $a_{\perp}$, therefore show a thermal increase of $\Delta a_{\perp}(T)/a_{\perp}(20\,°C)$ between $\int \Delta\alpha\, dT$ for a complete thermal mismatch strain relaxation, and $(1+A)\int \Delta\alpha\, dT$ for a completely pinned interface.

Expressed as a rhombohedral distortion $\epsilon_r = \epsilon_{\parallel} - \epsilon_{\perp}$, $\epsilon_r = 0$ for a completely relaxed layer, while for a completely elastically strained layer $\epsilon_r = (1+A)\int \Delta\alpha\, dT$. Figure 5 shows a temperature dependence of the perpendicular lattice constant $\Delta a_{\perp}$ for a particular stack with a BaF_2 layer 2000 Å thick. Above RT, part of the strain relaxes.[27] In addition, hysteresis effects occur when cycling the temperature, as also reported for single SrF_2 and CaF_2 layers on Si(111).[29] Below RT, the points follow the pinned behavior within the measurement accuracy. No cracks or delaminations were observed after such cycling.

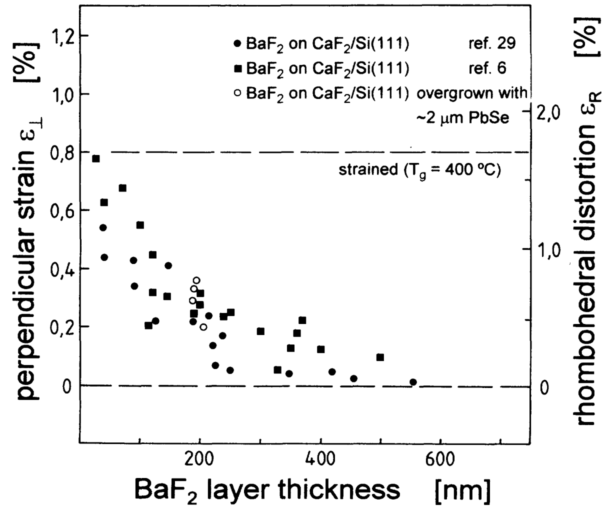

FIG. 4. Perpendicular strains in $BaF_2(111)$ layers grown on CaF_2/Si(111) with about 20 nm thickness of the intermediate CaF_2 buffer layer. Full symbols: BaF_2 top layers; open symbols: strain in BaF_2 layers overgrown with PbSe.

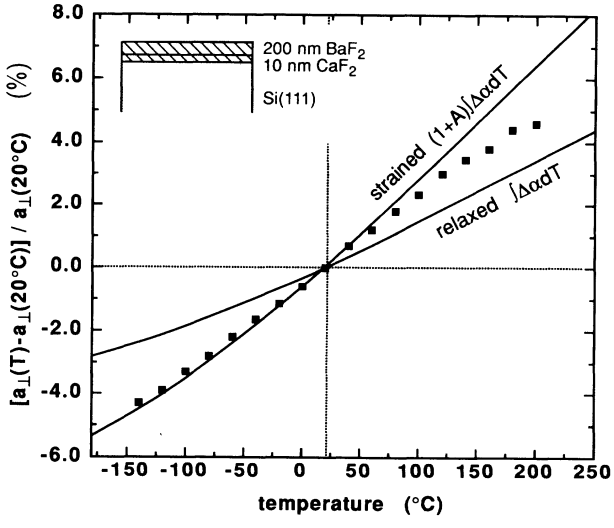

FIG. 5. Lattice spacings of a 2000-Å-thick $BaF_2(111)$ layer on CaF_2/Si(111) vs temperature. The expected behavior for a completely relaxed and completely elastically strained layer is indicated, too.

C. PbSe on $BaF_2/CaF_2/Si(111)$

1. Strain relaxation at low temperatures

In contrast to BaF_2, PbSe relaxes the thermal mismatch strain even at cryogenic temperatures. Figure 6 shows the rhombohedral distortion ϵ_r of PbSe layers of different thicknesses as a function of temperature. The measurements were performed within one single cooldown cycle. The strain level remains nearly constant down to the lowest temperature, i.e., nearly no additional thermal mismatch strain can build up. The strain value as a function of the layer thickness d shows the approximate $1/d$ dependence predicted by Matthews's theory. However, the absolute values calculated from the theory with published elastic constants are about six times lower than measured.

The strain state of the underlying BaF_2 is not affected by the PbSe overgrowth. As determined with the Bond method, the strain of the BaF_2 buffer is relaxed at RT; the remaining strain $\epsilon_\perp$ is between 0.2% and 0.4% (Fig. 4), i.e., the same values as for BaF_2 layers which are not overgrown.

2. Strain relaxation after many temperature cycles

Figure 7 shows schematically the strain expected in PbSe layer after growth on cooldown to low temperatures, and cycling the layer between RT and a still lower temperature. The compressive strain remaining after growth is almost completely relaxed before cooldown for layers with about 2 μm thickness as used for the experiment. Decreasing the temperature, the strain first follows the "elastic limit;" the layer deforms only elastically. As soon as the critical resolved shear stress for dislocation glide is exceeded, the strain remains nearly constant or increases only slightly on further cooldown because the work hardening is low. Increasing the temperature after having reached the lowest temperature, the strain first follows the slope of the elastic limit since the tensile strain of the layer decreases due to the higher thermal-expansion coefficient of the overgrowth. On further temperature increase, the strain becomes compressive. When it exceeds the critical shear stress for glide under a compressive stress, strain relaxes by dislocation glide. The compressive strain remains nearly constant or increases slightly until the highest temperature is reached. When cooling down again, the layer deforms elastically until the critical shear stress on the tensile side is reached before it starts to relax again.

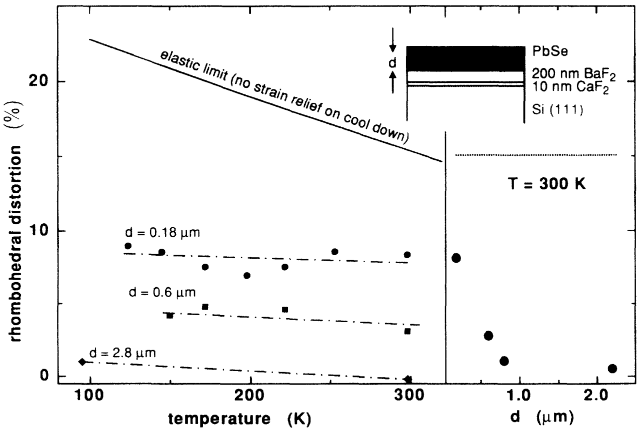

FIG. 6. Rhombohedral distortion ϵ_r for PbSe(111) layers on $BaF_2/CaF_2/Si(111)$ vs thickness (right) and at different temperatures (left). Without strain relaxation after growth, the experimental points would follow the indicated slope of the elastic limit.

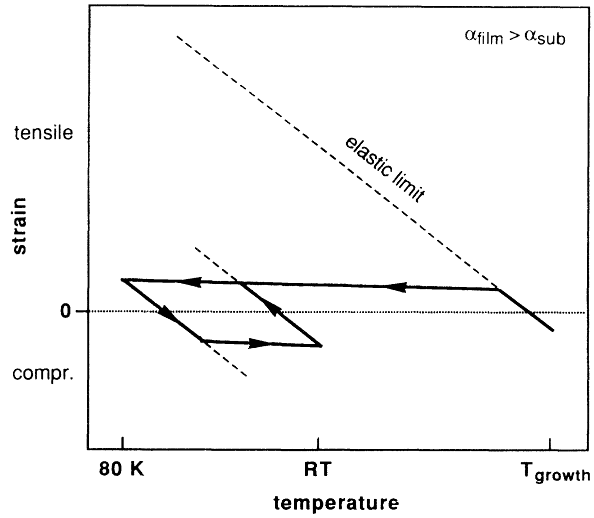

FIG. 7. Schematic behavior of the thermal mismatch strain in PbSe on Si(111) layers vs temperature change.

This behavior is observed experimentally as shown in Fig. 8(a). The change in strain was obtained by determining the change in $a_\perp$ using XRD with symmetric (444) reflections. Starting at the lowest temperature, the change in strain was measured at different temperatures on going up to RT, followed by a cooldown. The observed change of the rhombohedral distortion ϵ_r between the lowest and highest values for this cycle between RT and -150 °C is about $\Delta\epsilon_{r,\mathrm{meas}} \approx 0.2\%$, while for purely elastic behavior, the change in ϵ_r would be as high as

$$\Delta\epsilon_{r,\mathrm{el}} = (1+A)\int \Delta\alpha\, dT \approx (1+1.16)\times 0.38\,\% = 0.82\%$$

for cycling between RT and 77 K. Most of the strain induced by the thermal mismatch is therefore relaxed by movement of dislocations even at cryogenic temperatures. The measured maximal absolute value of ϵ_r is below about 2×10^{-3}, which corresponds to a maximal biaxial parallel strain $\epsilon_\parallel$ of $\approx 1\times 10^{-3}$. The corresponding biaxial stress is $\sigma_\parallel = 69$ MPa from which a value of $S\sigma_\parallel \approx 32$ MPa ($S = 0.47$ is the Schmid factor) follows for the resolved shear stress. This is a rather low value compared to III-V or II-VI semiconductors, but still a factor of 20 higher than the critical resolved shear stress reported for PbS single crystals at RT, $\sigma = 1.4$ MPa,[30] oriented for single glide and probably starting with a much lower dislocation density (no values for PbSe single crystals are presently available to our knowledge).

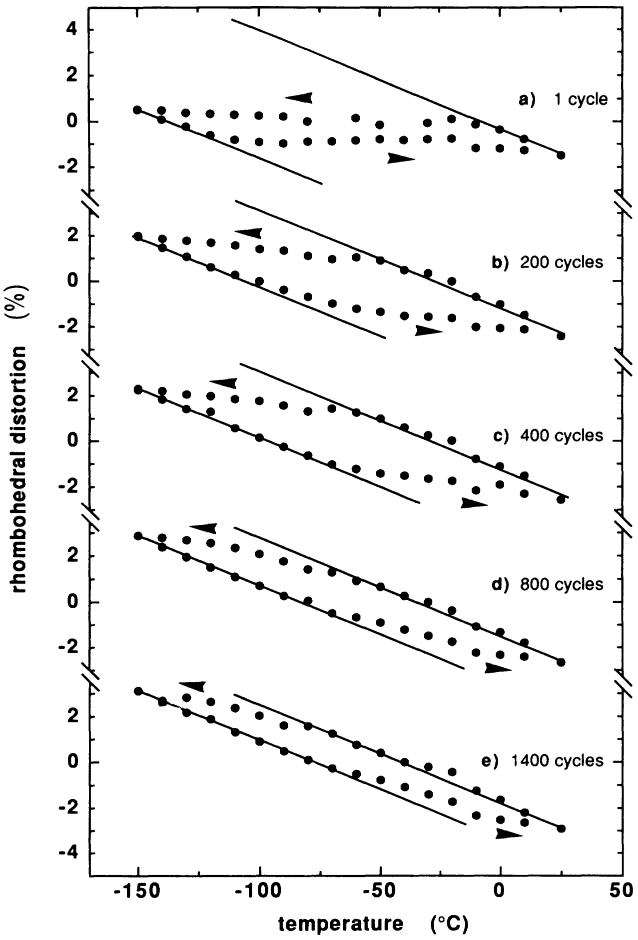

FIG. 8. Measured strain in a 3-μm-thick PbSe(111) layer on $BaF_2/CaF_2/Si(111)$ during a temperature cycle down to cryogenic temperature after (a) 1, (b) 200, (c) 400, (d) 800, and (e) 1400 cycles. Without plastic relaxation by dislocation glide, the points follow the slope of the indicated full lines (elastic limit).

Up to about 20 such temperature cycles, no significant changes are observed in the hysteresis curves. Many more cycles are needed to study a possible deformation hardening. Figures 8(b)–8(e) show the hysteresis curves obtained with the same PbSe sample after it had undergone 200, 400, 800, and 1400 cycles between room temperature and 77 K. The hysteresis curve widens somewhat with increasing number of cycles, as larger tensile and compressive strains occur owing to deformation hardening. After 200 cycles, $\Delta\epsilon_{r,\mathrm{meas}}$ increased to about 0.4%, slightly increases further with continued cycling, and reaches $\Delta\epsilon_{r,m}\approx 0.6\%$ after 1400 cycles. Therefore, even after 1400 cycles, the highest number we performed up to now, $(0.82-0.6)\%=0.22\%$ plasticity still occurs on each cycle. The total cumulative plastic deformation the layer has undergone after 1400 cycles is $\epsilon_{\parallel,\mathrm{tot}}=\sum(|\epsilon_{\parallel,\mathrm{el}}-\epsilon_{\parallel,\mathrm{meas}}|)$ summed over all cycles with the appropriate values of $\epsilon_{\parallel,\mathrm{meas}}=\epsilon_{r,\mathrm{meas}}/(1+A)$ as a function of the number of cycles inserted. The numerical value is about 4; the total cumulative plastic relaxation the layer has undergone is as high as about 400%. The layer withstands this cyclic plastic deformation without showing cracks or delamination.

The hysteresis after 1400 cycles has considerably narrowed due to the deformation hardening. If cycling were continued further, the hysteresis would get smaller and smaller until the final strain vs temperature curve would become completely elastic. However, the point of zero strain would now lie symmetrically between the highest and lowest temperatures of the cycling experiments; the strain would be about 0.4% compressive at RT, zero at about 190 K, and about 0.4% tensile at 77 K. Since no cracks were observed in the cycled layers, which suffered, according to Fig. 8(e), a maximal compressive or tensile strain of 0.3%, it seems reasonable to conclude that the layer would withstand a fully elastic deformation, too, since the corresponding maximal strain would be only 25% higher than after 1400 cycles, and the point of zero strain remains symmetrically between the extreme temperature excursions.

3. *HRXRD and dislocation density*

HRXRD was performed after different numbers of cycles to study the change of defect densities. The full width at half maximum (FWHM) of the curves vs the number of temperature cycles is shown in Fig. 9. A slight increase in the FWHM with the number of cycles is observed; the FWHM is about 140 arc sec before and $\approx$200 arc sec after 1400 cycles. However, this change lies within the scatter between different positions of typical samples with 3-in. diameter as obtained after growth. Figure 10 shows a rocking curve of the sample after 1400 cycles.

The density of threading dislocations can be estimated from the measured FWHM. Assuming a Gaussian distribution, the analysis from Ayers allows one to estimate the dislocation densities by two independent methods.[31]

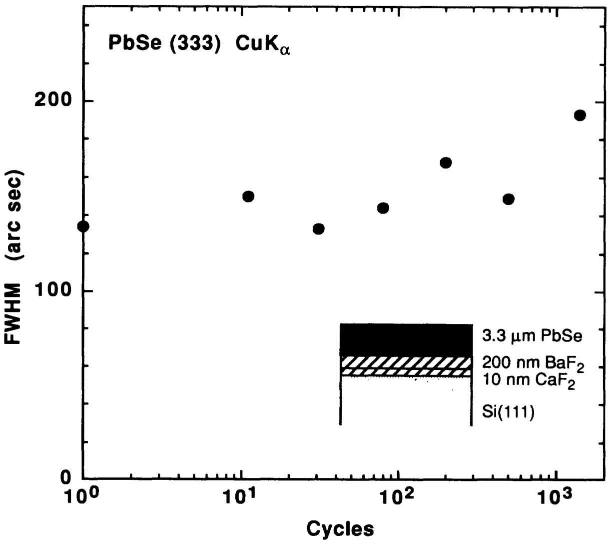

FIG. 9. Linewidths (FWHM, 333 line excited with Cu $K\alpha$) of HRXRD rocking curves of 3-μm-thick PbSe(111) layers on $BaF_2/CaF_2/Si(111)$ vs the number of temperature cycles between RT and 77 K.

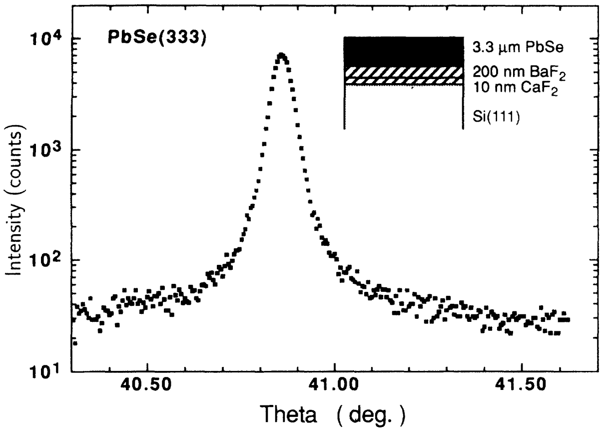

FIG. 10. HRXRD rocking curve (333 line excited with Cu $K\alpha$) of a 3.3-μm-thick PbSe(111) layer on BaF_2/CaF_2/Si(111) after 1400 cycles between RT and 77 K.

By plotting the measured FWHM for different reflections vs $\tan^2\theta$ where θ is the Bragg angle, a straight line should result. The dislocation density ρ (in cm^{-2}) is obtained either from the intercept K_α of the line with the ordinate by

$$\rho = K_\alpha / 4.36 b^2$$

or from the slope K_ϵ by

$$\rho = K_\epsilon / \{0.09 b^2 |\ln(2\times 10^{-7}\rho)|\} ,$$

where **b** is the Burgers vector.

Figure 11 shows this plot for the sample after 1400 cycles. The dislocation density obtained from the intercept method is 8×10^7 cm^{-2}, while the slope method yields 1.2×10^8 cm^{-2}. For the calculations, screw dislocations were assumed. Assuming edge dislocations would change the values only slightly.

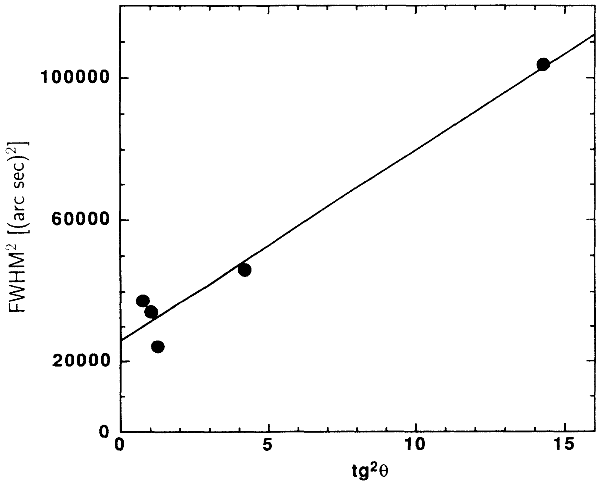

FIG. 11. Drawing according to Ayers (Ref. 31) of FWHM vs Bragg angle for the PbSe layer on Si cycled 1400 times between RT and 77 K. The dislocation densities estimated from the intercept or slope of the fitted straight line are about 10^8 cm^{-2}.

Both numbers are consistent within the accuracy to be expected from the theory. Dislocation densities were analyzed with the same type of samples (without temperature cycling) grown under similar conditions with TEM by Mathet *et al.*,[9] too. They observed densities at the surface somewhat below 10^7 cm^{-2}. These values are comparable to our values, since dislocation densities are lowest at the surface, while the HRXRD linewidth yields a weighted mean over the whole 3-μm-thick layer.

The mean spacing of the part of the dislocations relieving thermal misfit before temperature cycling was $s = 160$ nm as determined with STM.[7,8] This corresponds to a change in strain of 0.5% on cooling from growth to RT due to the thermal mismatch. Assuming that each misfit dislocation consists of a misfit part of length l and two threading ends extending up to the surface, the number of intersections ρ of these threading ends with the surface is correlated with s and l by $ls\rho = 6$ for threefold symmetry.[6] With $\rho = 10^8$ cm^{-2} and $s = 160$ nm, l is therefore about 40 μm. This is a lower estimate, since an appreciable number of threading dislocations are sessile and originate from other causes than from glissile dislocations relieving thermal mismatch. If the more realistic value $\rho = 10^7$ cm^{-2} is chosen,[9] l amounts to 400 μm as a lower estimate.

4. *Discussion of dislocation glide after many thermal cycles*

If all strain relaxation for an additional temperature cycle from RT to 77 K and back [change in thermal expansion difference of $(2\times 0.38)\%$] occurs by formation of *new* dislocations, the spacing between these new dislocations is $s \approx 110$ nm.[8] The lengths l of these new dislocations must be much larger than the 40–400 μm deduced above in order that the threading dislocation density does not appreciably increase after each temperature cycle, in order not to contradict the HRXRD results. On the other hand, according to the STM results of a cycled sample (Fig. 2), new dislocations have formed and glided through the crystal at least after the first cycle. A spacing of 110 nm corresponds to about 300 atomic layers. Thus, at least after 300 cycles down to 77 K, new dislocations have to glide on the *same* atomic glide planes as those dislocations which already have moved through. If the lengths l of the dislocations which already have moved through is longer than the dimensions of the sample (≈ 10 mm), new dislocations have to be formed. However, it is rather to be expected that most of the dislocations which have already moved through the layer have shorter lengths, so that their threading ends are still available for new movements. In this case, no new dislocations need be created. Continued cycling therefore means that after some cycles no new dislocations are formed, but the same dislocations move back and forth across the layer thickness to relieve the strain. Since the observed threading dislocation density does not increase appreciably on cycling, dominance of back and forth glide of the threading ends of the same dislocations most probably already occurs after the first few cycles. The mean distance they move is reduced after many cycles owing to strain hardening. If the production rate of obstacles which hinder glide is low enough, no rapid deformation hardening occurs, as observed.

5. Temperature cycling with other layer combinations

Temperature cycling of the following stacks was also investigated:

(i) $Pb_{1-x}Sn_xSe$ on $BaF_2/CaF_2/Si$,
(ii) PbTe on $BaF_2/CaF_2/Si$,
(iii) SiO_2 on PbSe on $BaF_2/CaF_2/Si$, and
(iv) PbSe on CaF_2/Si.

For each of these stacks, the IV-VI layer was about 3 μm thick, the thickness of the BaF_2 was about 200 nm and that of the CaF_2 about 10 nm, and all layers were (111) oriented. These stacks were cycled up to 500 times between RT and 77 K. Hysteresis curves of strain and the FWHM of rocking curves were determined. Stack (i) was chosen to investigate the effect of solid-solution hardening due to the substitution of Pb by Sn. For stack (ii), the lattice mismatch with BaF_2 is larger, but it is known that PbTe behaves similarly to PbSe, or is even softer. Therefore not much change compared to PbSe layers is expected. In stack (iii), the PbSe layer was overgrown with about 200 nm amorphous SiO_2 at RT. SiO_2 has a much smaller thermal-expansion coefficient than PbSe, its thermal expansion being comparable to that of the Si substrate. This sample served as a test to find out whether a SiO_2 cap layer hinders the creation and/or movement of strain-relieving dislocations in the PbSe main layer. Finally, stack (iv) was tested, where a very thin CaF_2 buffer layer only serves for compatibility. This stack is most interesting for infrared sensor fabrication, since the omission of the BaF_2, which is soluble in water, greatly facilitates microlithography by wet etching.[13]

For all stacks (i)–(iv), similar results as with the PbSe sample described in detail above were obtained: no delamination or crack formation, the hysteresis curves show only slight deformation hardening, and no significant increase of the FWHM of x-ray rocking curves.[21] The formation and movement of dislocations relieving thermal misfit strain works, therefore, in the same manner for PbTe and is not significantly hindered in ternary $Pb_{1-x}Sn_xSe$ by solid-solution hardening or by an overgrowth like SiO_2.

V. CONCLUSIONS

The strain induced by the thermal mismatch in stacks of $PbSe/BaF_2/CaF_2$ and BaF_2/CaF_2 on Si(111) substrates relaxes by movement of dislocations gliding in the main $\langle 110\rangle\{100\}$ glide system of the layers. After the misfit part of such a dislocation has moved across the whole layer on its inclined glide plane, no defect is left, but only a surface step is created. The strain relief is not affected whether the corresponding layer is at the top of the stack or is covered by another layer of the stack materials. The formation of new dislocations or the glide of already existing ones is therefore not hindered by the overgrowth. The thermal mismatch strain relaxes down to approximately RT for the BaF_2 and CaF_2 layers, while these layers strain completely elastically below RT. PbSe(111) layers are capable of relieving most of the thermal mismatch strain even at 77 K, and plasticity occurs even after many temperature cycles between RT and 77 K. After 1400 such cycles, still about 25% of the elastic strain induced by the difference in thermal expansion between the PbSe layer and the Si substrate relaxes by dislocation glide on each cycle. HRXRD rocking curves from the 3-μm-thick PbSe layers are 150–200 arc sec wide. Only a slight broadening is observed with increasing number of cycles, although the cumulative plastic deformation of the layer reaches a value as high as 400%. The layers maintain their quality because after some initial thermal cycles essentially no new dislocations are created, but the existing ones move back and forth on the same atomic glide plane with each cycle. The temperature where zero strain occurs lies midway between RT and 77 K after the first cycles; the layers are under a compressive strain at RT, while a tensile strain of approximately the same magnitude prevails at 77 K. No cracks or delamination were observed. If cycling were continued, a fully elastic behavior would occur at the end owing to strain-hardening effects. However, since the change in strain is now symmetrized and would increase by not more than 25% for a pure elastic behavior, it is expected that even in this case the layers would withstand the induced strains without problems. The same behavior was observed for $Pb_{1-x}Sn_xSe$ layers on Si (suited for infrared sensors with cutoff wavelengths above 7 μm), and also for layers which are overgrown with a dielectric cap with thermal-expansion coefficient comparable to that of Si for insulating purposes. Even if other IV-VI materials with higher deformation hardening were chosen and if they can be cooled down to cryogenic temperature without cracking, further cooling cycles become less critical due to the strain symmetrization effect on heating up to RT. The PbSe and other IV-VI layers therefore maintain their quality for infrared device fabrication regardless of the number of temperature cycles.

ACKNOWLEDGMENTS

The financial support of the Swiss National Science Foundation (NFP24) is gratefully acknowledged. The authors thank Dr. R. E. Pixley for the RBS work and for a critical reading of the manuscript.

---

[1] E. A. Fitzgerald, Mater. Sci. Rep. **7**, 87 (1991).

[2] N. A. El-Masry, J. C. L. Tarn, and S. M. Bedair, Appl. Phys. Lett. **55**, 1442 (1989).

[3] F. K. LeGoues, B. S. Meyerson, and J. F. Morar, Phys. Rev. Lett. **66**, 2903 (1991).

[4] This is true for an infinitely extended layer. With patterned structures, a slightly inclined stress field results, which might possibly be able to move dislocations in a plane parallel to the interface.

[5] S. Blunier, H. Zogg, C. Maissen, A. N. Tiwari, R. M. Overney,

H. Haefke, P. A. Buffat, and G. Kostorz, Phys. Rev. Lett. **68**, 3599 (1992).

[6] S. Blunier, Ph.D. thesis, Swiss Federal Institute of Technology, 1992.

[7] H. Zogg, C. Maissen, S. Blunier, S. Teodoropol, R. M. Overney, T. Richmond, and J. W. Tomm, Semicond. Sci. Technol. **8**, S337 (1993).

[8] C. Maissen, Ph.D. thesis, Swiss Federal Institute of Technology, 1992.

[9] V. Mathet, P. Galtier, F. Nguyen-Van-Dau, G. Padeletti, and J. Olivier, J. Cryst. Growth **132**, 241 (1993).

[10] Véronique Mathet, Ph.D. thesis, Univèsité de Paris Sud, Centre d'Orsay, 1993.

[11] F. Nguyen-Van-Dau, V. Mathet, P. Galtier, G. Padeletti, J. Olivier, D. G. Crété, and P. Collot, Mater. Sci. Eng. **B21**, 317 (1993).

[12] H. Zogg, S. Blunier, T. Hoshino, C. Maissen, J. Masek, and A. N. Tiwari, IEEE Trans. Electron. Devices **38**, 1110 (1991).

[13] H. Zogg, A. Fach, C. Maissen, J. Masek, and S. Blunier, Opt. Eng. **33**, 1440 (1994).

[14] J. Masek, Ph.D. thesis, Swiss Federal Institute of Technology, 1994.

[15] W. A. Jesser and J. H. van der Merwe, J. Appl. Phys. **75**, 872 (1994).

[16] W. L. Bond, Acta Crystallogr. **13**, 814 (1960).

[17] S. Blunier, V. Meyer, R. E. Pixley, H. Stüssi, S. Teodoropol, and H. Zogg, Nucl. Instrum. Methods Phys. Res. Sect. B **63**, 56 (1992).

[18] R. E. Pixley (unpublished).

[19] W. J. Bartels, J. Vac. Sci. Technol. B **1**, 338 (1983).

[20] H. Zogg, S. Blunier, and J. Masek, J. Electrochem. Soc. **136**, 775 (1989).

[21] S. Teodoropol, Ph.D. thesis, University of Zürich, 1994.

[22] J. W. Matthews, in *Dislocations in Solids,* edited by F. R. N. Nabarro (North-Holland, Amsterdam, 1989), Vol. 2, p. 461.

[23] J. Petruzzello, B. L. Greenberg, D. A. Cammack, and R. Dalby, J. Appl. Phys. **63**, 2299 (1988).

[24] L. J. Schowalter and W. Li, Appl. Phys. Lett. **62**, 696 (1993).

[25] S. Hashimoto, J.-L. Peng, W. M. Gibson, L. J. Schowalter, and R. W. Fathauer, Appl. Phys. Lett. **47**, 1071 (1985).

[26] We do not see any evidence that the strain in CaF_2 layers drops much faster above a layer thickness of 1700 Å as stated by these authors. Such a drop possibly can be caused by cracks in the layers which become visible after etching only, since the tendency to form cracks increases dramatically with increasing layer thickness.

[27] H. Zogg, Appl. Phys. Lett. **49**, 933 (1986).

[28] S. Blunier, H. Zogg, and A. Rüegge, Thin Solid Films **184**, 387 (1990).

[29] W. Li, S. Hymes, S. P. Murarka, and L. J. Schowalter, in *Thin Films: Stresses and Mechanical Properties IV,* edited by P. H. Townsend, T. P. Weihs, J. Sanchez, Jr., and P. Børgesen, MRS Symposia Proceedings No. 308 (Materials Research Society, Pittsburgh, 1993).

[30] P. Haasen, Mater. Sci. Technol. **1**, 1013 (1985).

[31] J. E. Ayers, J. Cryst. Growth **135**, 71 (1994).

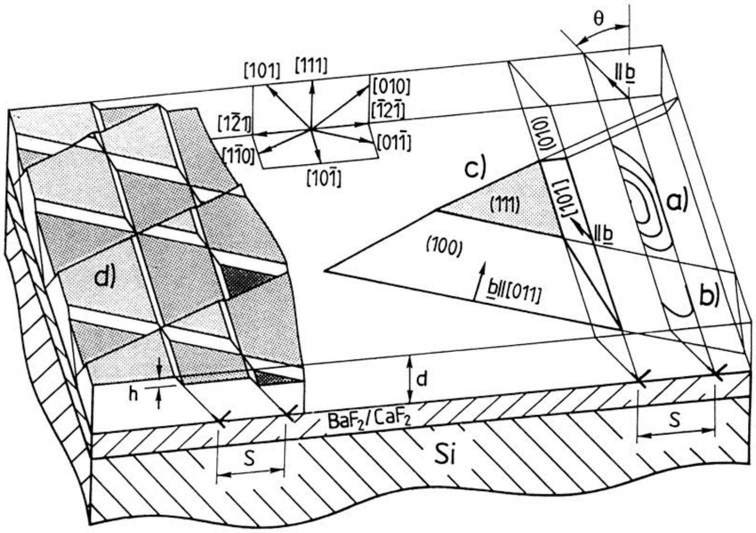

FIG. 1. Schematic drawing of nucleation (a) and glide of thermal-misfit-strain-relieving dislocations (b), glide planes and Burgers vectors of the $\langle 110 \rangle \{100\}$ glide system for (111) oriented layers (c), and the resulting surface terrace morphology (d).

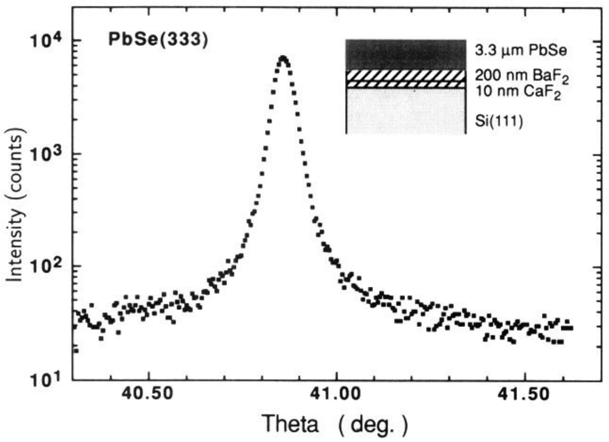

FIG. 10. HRXRD rocking curve (333 line excited with Cu $K\alpha$) of a 3.3-μm-thick PbSe(111) layer on $BaF_2/CaF_2/Si(111)$ after 1400 cycles between RT and 77 K.

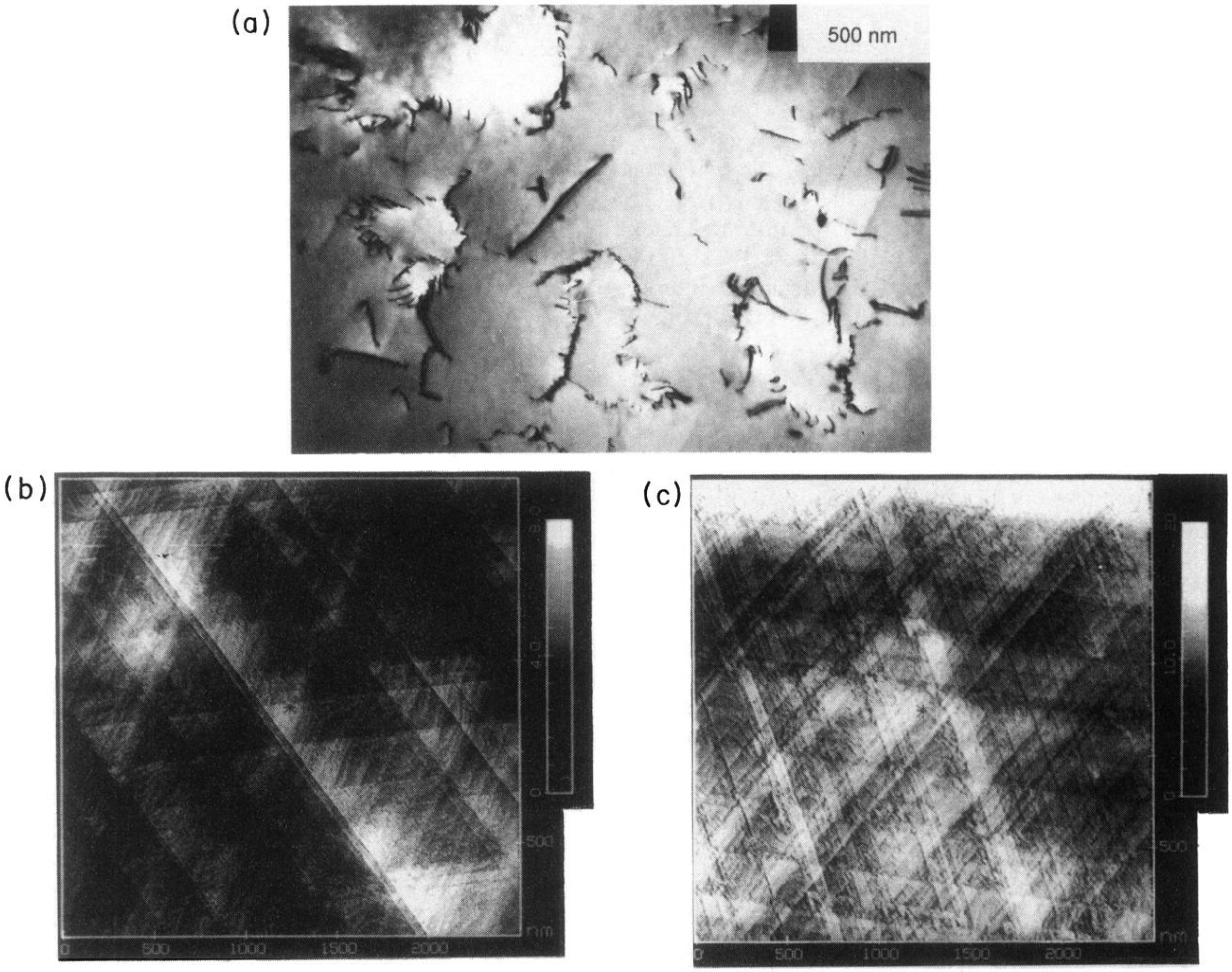

FIG. 2. (a) TEM image of a 0.2-μm-thick PbSe layer dissolved from the $BaF_2/CaF_2/Si(111)$ substrate. The main contrast is from threading dislocations. (b) STM image of a 2-μm-thick PbSe layer on $BaF_2/CaF_2/Si(111)$. The straight slip steps run along the three $\langle 011 \rangle$ directions, the intercepts of the $\{100\}$ glide planes with the surface. (c) Same sample as in (b), but after a temperature cycle down to 77 K.

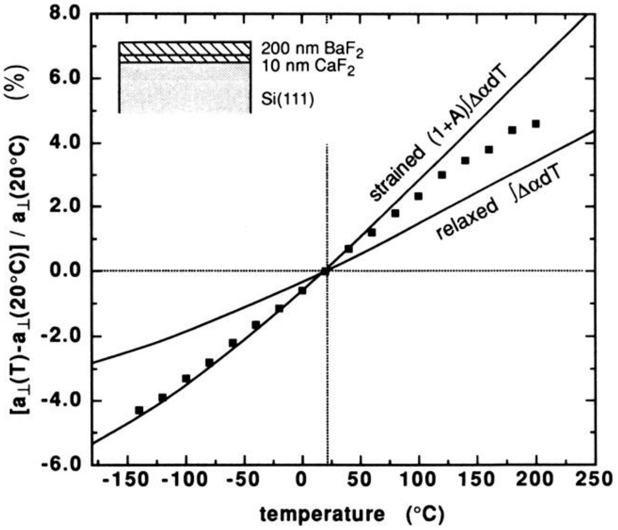

FIG. 5. Lattice spacings of a 2000-Å-thick $BaF_2(111)$ layer on $CaF_2/Si(111)$ vs temperature. The expected behavior for a completely relaxed and completely elastically strained layer is indicated, too.

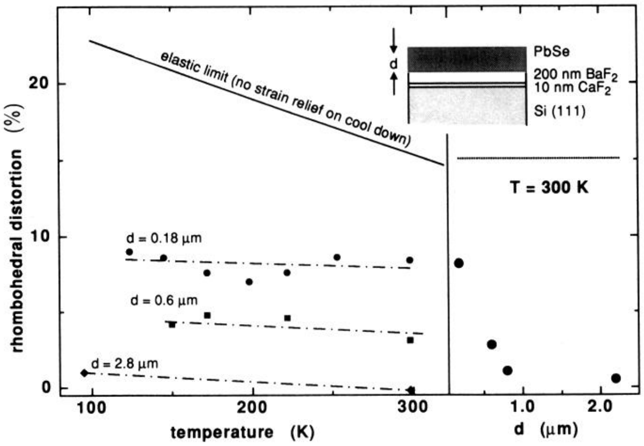

FIG. 6. Rhombohedral distortion ϵ_r for PbSe(111) layers on $BaF_2/CaF_2/Si(111)$ vs thickness (right) and at different temperatures (left). Without strain relaxation after growth, the experimental points would follow the indicated slope of the elastic limit.

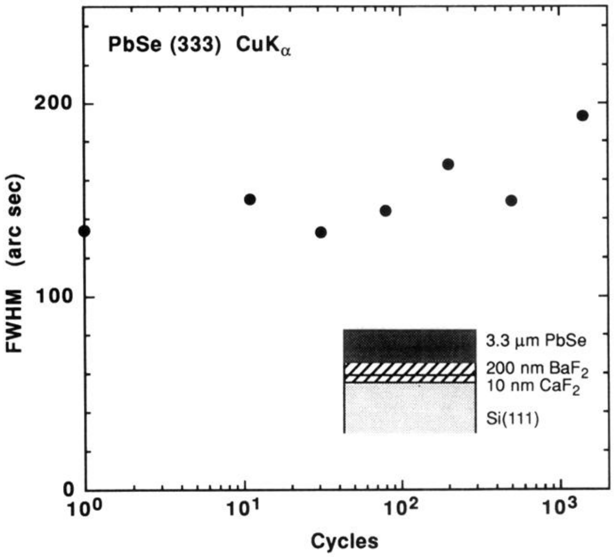

FIG. 9. Linewidths (FWHM, 333 line excited with Cu $K\alpha$) of HRXRD rocking curves of 3-μm-thick PbSe(111) layers on $BaF_2/CaF_2/Si(111)$ vs the number of temperature cycles between RT and 77 K.